

Investigating the nature of narrow-line Seyfert 1 galaxies with high-energy spectral complexity

L. C. Gallo

Max-Planck-Institut für extraterrestrische Physik, Postfach 1312, 85741 Garching, Germany

Institute of Space and Astronautical Science, Japan Aerospace Exploration Agency, Yoshinodai 3-1-1, Sagami-hara, Kanagawa 229-8510, Japan

Accepted. Received.

ABSTRACT

With the commissioning of *XMM-Newton* came the discovery of 2.5 – 10 keV spectral complexity in some narrow-line Seyfert 1 galaxies (NLS1). This high-energy complexity can be manifested as sharp, spectral drops or gradual curvature in the spectrum. Models which are normally considered are ionised reflection and partial-covering. In this work, we define two samples of NLS1: a complex sample whose members exhibit high-energy complexity (C-sample), and a general sample of NLS1 whose 2.5 – 10 keV spectra do not strongly deviate from a simple power law (S-sample). We then compare multiwavelength parameters of these two samples to determine if there are any distinguishing characteristics in the complex NLS1. Considering historical light curves of each object we find that the C-sample is representative of NLS1 in a low X-ray flux state, whereas the members of the S-sample appear to be in a typical flux state. Moreover, from measurements of α_{ox} with contemporaneous UV/X-ray data, we find that the C-sample of NLS1 appear X-ray weaker at the time of the observation. For two NLS1 in the C-sample multi-epoch measurements of α_{ox} are available and suggest that α_{ox} approaches more normal values as the complexity between 2.5 – 10 keV diminishes. This implies that a source could transit from one sample to the other as its X-ray flux varies. Secondly, there are indications that the C-sample sources, on average, exhibit stronger optical Fe II emission, with the three most extreme (Fe II/H β > 1.8) Fe II emitters all displaying complexity in the 2.5 – 10 keV band. It is an intriguing possibility that we may be able to identify X-ray complex NLS1 based on the extreme strength of the more easily observable optical Fe II emission. However, it is not clear if the possible connection between Fe II strength and spectral complexity is due to the Fe II producing mechanism or because strong Fe II emitters may exhibit the greatest variability and consequently more likely to be caught in an extreme (low) flux state. Based on the current analysis it we can not straightforwardly dismiss absorption or reflection as the cause of the X-ray complexity; by considering the multiple UV/X-ray observations of 1H 0707–495 (a C-sample member), we discuss a possible method of distinguishing the two models provided further UV/X-ray observations.

Key words: galaxies: active – galaxies: nuclei – X-ray: galaxies

1 INTRODUCTION

The importance of narrow-line Seyfert 1 galaxies (NLS1) became apparent on the discovery of the ‘primary eigenvector’ (PC1; Eigenvector 1) in the Boroson & Green (1992) principle component analysis of PG quasars. PC1 showed a strong anticorrelation between the strengths of [O III] and Fe II in the optical spectra, with NLS1 as a class showing the strongest Fe II emission and weakest [O III]. While the physical driver of PC1 is still debated, there are strong indications that the fraction of the Eddington luminosity (L/L_{Edd}) at which the object is emitting at is responsible, implying that NLS1 are relatively high accretion rate systems. Since there are no significant differences between NLS1 and broad-line Seyfert

1 galaxies (BLS1) in their X-ray, optical, or bolometric luminosities (Grupe et al. 2004), it naturally follows from the condition of higher accretion rates that NLS1 possess a lower mass black hole compared to BLS1 of similar luminosity. Black hole mass measurements confirm lower mass black holes in NLS1 (Wandel, Peterson & Malkan 1999; Peterson et al. 2000; Grupe & Mathur 2004).

The strong Fe II emission in NLS1 is prevalent in the UV (e.g. Laor et al. 1997; Constantin & Shields 2003), optical (e.g. Boroson & Green 1992), and infrared (e.g. Rodríguez-Ardila et al. 2002). The observed line widths and absence of forbidden emission suggests that Fe II is formed in the dense BLR, but photoionisation models cannot account for all of the Fe II emission. The ‘Fe II discrepancy’ remains unsolved, though models which consider non-

radiative heating (probably due to shocks produced in outflows), with an overabundance of iron are promising (see Collin & Joly 2000 for a review).

Perhaps the most interesting characteristics of NLS1 are manifested in the X-ray regime. The origin of the strong soft excess emission below about 1 keV, known since *Einstein* observations (e.g. Puchnarewicz et al. 1992; see also Boller, Brandt & Fink 1996), is still debated (e.g. Mineshige et al. 2000; Gierlinski & Done 2004; Crummy et al. 2005); as is the nature of the extreme, rapid variability. With *ASCA*, came the discovery that the 2 – 10 keV spectrum in NLS1 also appeared steeper than in BLS1 (Brandt, Mathur & Elvis 1997). The result could be understood as arising from significant Compton cooling of the accretion disc corona due to the strong soft X-ray excess found in most NLS1. The lower energy gain per scattering (smaller Compton y parameter) would yield steeper, hard X-ray slopes.

With the high-sensitivity of *XMM-Newton* came what may be the most interesting discovery with regards to NLS1, and that was the presence of a sharp, spectral drop at $E = 7$ keV in 1H 0707–495 (Boller et al. 2002). Since then, a number of drops at $E \gtrsim 7$ keV (or more generally ‘high-energy curvature’) have been observed in several NLS1 (e.g. Pounds et al. 2003, 2004; Longinotti et al. 2003; Boller et al. 2003; Uttley et al. 2004; Reeves et al. 2004). The exact nature of this behaviour, which seems to be a characteristic of NLS1, is uncertain. Two models which appear probable are partial-covering (e.g. Tanaka et al. 2004 and references within) and reflection (e.g. Fabian et al. 2002).

In terms of partial-covering, the ~ 7 keV drop is produced by absorption of the continuum emission by a dense material, which only partly obscures the primary emitter. This can, in principle, explain the absence of other absorption features (e.g. intrinsic cold absorption, Fe L absorption, fluorescence emission), and if the absorber is allowed to be in radial motion, it can possibly account for the various edge energies which are seen (e.g. Gallo et al. 2004a). It is important to realise that partial-covering does not describe the nature of the primary continuum source. Although a simple blackbody plus power law continuum is often assumed, other physical descriptions of the primary continuum are not dismissed, nor do they discriminate against partial-covering.

Reflection of the power law continuum source off the cold accretion disc can also adequately describe the X-ray spectra of NLS1 (e.g. Fabian et al. 2004). In this case, the sharp drop at high energies is the blue wing of a relativistically broadened iron line. In combination with light bending effects close to the black hole (e.g. Miniutti & Fabian 2004), the reflection model nicely describes the shape of the X-ray continuum and the principle of ‘reflection dominated’ spectra.

It stands to reason that regardless of the correct model, the process may be ubiquitous in NLS1 and probably in active galactic nuclei (AGN). By varying the prevalence of the physical process (e.g. the degree of absorption or amount of reflection) one can potentially describe the different types of X-ray spectra that are observed. Objects, such as IRAS 13224–3809 or 1H 0707–495, manifest ‘the process’ significantly; thus exhibiting sharp and deep spectral drops. Other NLS1, like NGC 4051, demonstrate the process only moderately, only displaying gentle curvature over the hard X-ray band. In most other NLS1, the process is minimal and likely not detected.

In this work we examine what, if anything, is unique about the NLS1 which appear to possess high-energy complexity. Leighly & Moore (2004) began to address this issue when they examined how the UV properties of IRAS 13224–3809 and 1H 0707–495 were re-

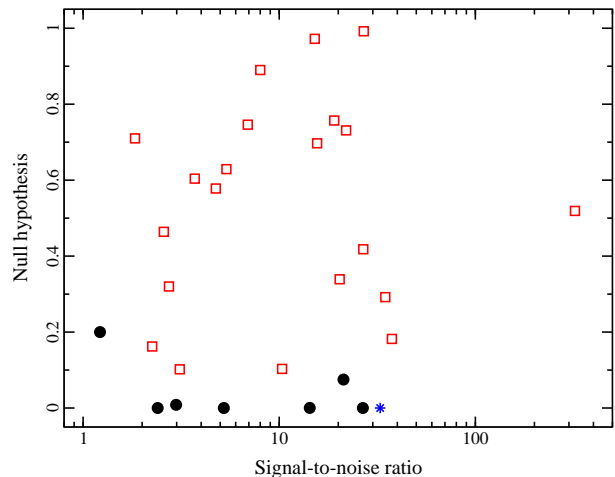


Figure 1. The null hypothesis of a power law plus Gaussian profile model to the intrinsic 2.5 – 10 keV spectrum of each NLS1 in the sample plotted against 5 – 10 keV SN. The filled (black) circles mark the NLS1 identified as complex (C-sample; see text for details). The open (red) squares are the general NLS1 sample (S-sample). MCG–6–30–15 is shown as a blue star for illustrative purposes.

markable compared to other NLS1. They found that IRAS 13224–3809 and 1H 0707–495 possessed weaker emission lines, significant asymmetry in the C IV profile and steeper spectra. They concluded that many of the differences in the two NLS1 could be explained in terms of radiative line driven wind models (e.g. Proga, Stone & Kallman 2000; Leighly 2004). Here, we continue to probe this issue by investigating multiwavelength properties of a sample of NLS1, which includes a larger number of ‘extreme’ objects.

The remainder of the paper is organised as follows. In the next section we define a complex sample of NLS1, which appear to exhibit high-energy complexity in their *XMM-Newton* (Jansen et al. 2001) spectra; and a general sample of NLS1, which do not show significant evidence of the complexity described here. In addition, the X-ray data processing is described. The dependence of X-ray flux state in defining the samples is investigated in Section 3. In Section 4, the calculation of the optical-to-X-ray spectral index from contemporaneous UV and X-ray data are described and presented. In Section 5 the multiwavelength parameters obtained from the literature (or estimated by us) are compared and our findings are highlighted. We discuss our results in Section 6 and give our summary in Section 7. A value for the Hubble constant of $H_0=70$ km s $^{-1}$ Mpc $^{-1}$ and a standard flat cosmology with $\Omega_M = 0.3$ and $\Omega_\Lambda = 0.7$ were adopted throughout.

2 X-RAY DATA PROCESSING AND SAMPLE DEFINITION

In defining a sample we considered all known NLS1 that have been observed on-axis and in imaging mode with the EPIC pn camera (Strüder et al. 2001) on *XMM-Newton*. The pn was selected to make use of what is most likely the highest signal-to-noise (SN), 2.5 – 10 keV rest-frame spectrum of these objects, currently available. At the time we commenced this study, there were more than 50 observations of 37 NLS1-type objects (including quasars and low-luminosity sources).

For each observation, the Observation Data Files (ODFs) were

Table 1. The X-ray data. The complete sample is divided into two sub-samples as described in the text. The information given is the: object name (column 1); observation data (column 2) and *XMM-Newton* revolution (column 3); total good exposure for the pn (column 4); observed 2.5 – 10 keV flux ($\times 10^{-11}$ erg cm $^{-2}$ s $^{-1}$) corrected for Galactic absorption (column 5); intrinsic 2 keV flux density ($\times 10^{-30}$ erg cm $^{-2}$ s $^{-1}$ Hz $^{-1}$) (column 6); null hypothesis from fitting the base model to the 2.5 – 10 keV data (column 7);

General NLS1 Sample (S-sample)						
(1) Source	(2) Date year.mm.dd	(3) <i>XMM-Newton</i> rev.	(4) pn exposure (ks)	(5) 2.5 – 10 keV flux	(6) 2 keV flux density	(7) Null Hypothesis
Mrk 766 ¹	2000.05.20	0082	26.0	1.33	19.08	0.757
Mrk 359	2000.07.09	0107	6.9	0.51	6.69	0.418
Mrk 1044	2002.07.23	0480	5.5	0.57	9.23	0.578
Akn 564 ^{1,2}	2000.06.17	0096	7.4	1.86	46.39	0.992
Mrk 896	2001.11.15	0355	7.2	0.31	5.08	0.339
Mrk 335	2000.12.25	0192	28.5	1.20	22.53	0.731
NGC 7158 ²	2001.11.27	0361	4.5	0.02	0.19	0.890
Mrk 493	2003.01.16	0568	13.3	0.31	5.95	0.629
I Zw 1	2002.06.22	0464	18.6	0.68	14.12	0.182
Ton S180 ¹	2000.12.14	0186	20.6	0.39	9.00	0.292
PG 1448+273	2003.02.08	0580	18.3	0.16	3.71	0.697
UGC 11763	2003.05.16	0629	26.2	0.31	3.46	0.102
RX J0323.2–4931	2003.08.16	0675	25.1	0.11	1.90	0.103
Mrk 478 ¹	2003.01.07	0564	18.2	0.15	2.98	0.972
II Zw 177 ²	2001.06.07	0274	8.7	0.08	2.09	0.604
IRAS 13349+2438	2000.06.20	0097	30.4	0.19	3.08	0.162
PKS 0558–504 ¹	2000.10.10	0153	8.0	1.03	20.75	0.519
PG 1115+407 ²	2002.05.17	0446	15.0	0.10	2.35	0.746
Nab 0205+024 ²	2002.07.23	0480	21.9	0.13	3.18	0.320
PG 2233+134 ²	2003.05.28	0635	7.5	0.05	1.15	0.713
E 1346+266 ²	2003.01.13	0567	49.2	0.005	0.47	0.464
Complex NLS1 Sample (C-sample)						
NGC 4051 ¹	2002.11.22	0541	44.7	0.59	4.98	< 0.01
PG 1535+547 ²	2002.11.03	0531	20.1	0.12	0.12	< 0.01
1H 0707–495 ¹	2000.10.21	0159	38.1	0.04	0.39	< 0.01
IRAS 13224–3809	2002.01.19	0387	54.3	0.04	0.84	< 0.01
PG 1211+143	2001.06.15	0278	49.5	0.27	3.24	< 0.01
PG 1402+261	2002.01.27	0391	9.1	0.15	3.30	0.09
PHL 1092 ²	2003.01.18	0570	19.8	0.02	0.31	0.20

FOOTNOTES: (1) Multiple *XMM-Newton* observations exist. (2) Adding an unresolved Gaussian profile was not an improvement over a simple power law fit.

processed to produce calibrated event lists using the *XMM-Newton* Science Analysis System (*XMM-SAS* v6.1.0) and the most recent calibration files. Unwanted hot, dead, or flickering pixels were removed as were events due to electronic noise. Event energies were corrected for charge-transfer losses, and time-dependent EPIC response matrices were generated using the *SAS* tasks ARFGEN and RMFGEN. Light curves were extracted from these event lists to search for periods of high background flaring, which were then removed. The source plus background photons were extracted from a source-centred circular region with a radius of 35''. The background was selected from an off-source region with a larger radius and appropriately scaled to the source region. Single and double events were selected for the pn spectra. Pile-up was examined in all spectra and when corrections were necessary the inner pixels of the source extraction region were ignored.

On processing of the spectral data, the sample was further refined by excluding observations in which: (i) the SN in the intrinsic 5 – 10 keV range was $\lesssim 1.2$, or (ii) the intrinsic 5 – 9 keV spectrum was not source dominated. Finally, if more than one observation of the same object was available, the highest SN data were used. This

filtering process resulted in the sample of 28 NLS1, which possess high-quality, intrinsic 2 – 10 keV spectra (Table 1).

The purpose of this study is to focus on the nature of NLS1 which exhibit complexity in their intrinsic ~ 2.5 – 10 keV spectra. To identify these objects, each spectra above 2.5 keV (rest-frame) was fitted with a baseline model composing of a power law modified by Galactic absorption (Dickey & Lockman 1990) plus, if necessary, an unresolved ($\sigma \lesssim 150$ eV) Gaussian profile between 6.4 – 7 keV. The intention of this baseline model was not to determine the ‘best-fit’ to the spectrum, but to identify the objects which, to first order, could not be explained by the most basic AGN model.

Sources for which the null hypothesis of this baseline model was < 0.10 were marked as NLS1 with high-energy complexity. We purposely adopted a low value for the null hypothesis to identify the most extreme cases which, in turn, should make it easier to identify other extreme characteristic of the sample. Six NLS1 (PG 1211+143, IRAS 13224–3809, 1H 0707–495, PG 1535+547, PG 1402+261 and NGC 4051) were categorised as having high-energy complexity. In addition, PHL 1092 was also included in this sub-sample because it exhibited a very flat, and likely unphysical,

2.5 – 10 keV power law ($\Gamma \approx 1.55$), even though the baseline model null hypothesis was 0.20. In total, seven objects make up the ‘complex NLS1 sample’ (hereafter C-sample). The remaining twenty-one sources compose the ‘general (simple) NLS1 sample’ (hereafter S-sample) (see Table 1).

Notably absent from the C-sample is the borderline NLS1, IRAS 13349+2438 ($\text{FWHM}(\text{H}\beta) \approx 2800 \text{ km s}^{-1}$, but strong Fe II emission; Grupe et al. 2004), which clearly shows high-energy complexity (Longinotti et al. 2003), but does not satisfy the rather strict criteria established here.

In Figure 1 the null hypothesis is plotted against the 5–10 keV SN for the objects in the sample. As will be adopted throughout, the filled circles will mark the members of the C-sample and the open squares will identify the S-sample population. The distribution of SN is comparable for the C- and S-sample. Therefore, even though identifying X-ray spectral complexity obviously depends on SN, it does not appear that it will be a significant bias in selecting our sample. For illustrative purposes the pn data for MCG–6-30-15 during revolution 302 are also included (blue star). We chose to include MCG–6-30-15 as it is perhaps the most obvious display of high-energy spectral complexity in a type 1 AGN.

3 X-RAY FLUX DEPENDENCE ON SAMPLE DEFINITION

We considered what effect X-ray variability could have on the sample definition by examining the historic 2 – 10 keV light curve for each object. Specifically, we compared the *XMM-Newton* X-ray fluxes measured for each object with past measurements from other missions.

ASCA fluxes were available either from Vaughan et al. (1999) or the TARTARUS archive for ten of the objects in the S-sample. Five objects also had *BeppoSAX* measurements (Comastri 2000) resulting in an X-ray flux measurement for eleven NLS1 in the S-sample (four having *BeppoSAX* and *ASCA* measurements). We found that for ten of them the flux varied by less than 50 per cent, although more typically on the 10 – 15 per cent level. This degree of variability is not abnormal for NLS1 on hourly time scales; therefore it seems that most members of the S-sample are in a typical flux state (of course, this is based on limited observations). The *XMM-Newton* flux of IRAS 13349+2438 diminished by more than ~ 70 per cent since the two *ASCA* observations. During the *BeppoSAX* observation, IRAS 13349+2438 was another ~ 70 per cent dimmer than during the *XMM-Newton* pointing. Due to our strict criteria, IRAS 13349+2438 has not been included in our C-sample, but it does appear to possess some high-energy complexity (Longinotti et al. 2003). It could be that in even lower flux states, such as that observed with *BeppoSAX*, the spectrum would appear even more complicated.

For three members of the C-sample, 1H 0707–495, NGC 4051 and PG 1211+143, it can be established from long-term, multi-mission light curves that the objects were in low-flux states during the *XMM-Newton* observations (see Leighly et al. (2002) for 1H 0707–495, Uttley et al. (2003, 2004) for NGC 4051, and Yaqoob et al. (1994) for PG 1211+143¹). Similarly, from a 10-day long *ASCA* observation (Dewangan et al. 2000) and comparison with the *BeppoSAX* observation (Comastri 2000) it can be shown

that IRAS 13224–3809 was also in an X-ray low-flux state during the *XMM-Newton* observation.

Data are sparse for PG 1535+547, PG 1402+261 and PHL 1092. Compared only to the *ASCA* fluxes, the *XMM-Newton* flux for PG 1535+547 was comparable while for PG 1402+261 it was ~ 40 per cent lower. For PHL 1092 the *XMM-Newton* flux was about 50 per cent lower than during the *ASCA* observation. It is difficult to determine if this indicates a low-flux state for PHL 1092. Variations of this order are typical on hourly time scales in the 0.1 – 2 keV range (Brandt et al. 1999; Gallo et al. 2004b); however the 2 – 10 keV variability is found to be negligible over similar time scales (Gallo et al. 2004b).

If not convincing, it appears rather suggestive that the S- and C-samples defined in this work are, by coincidence, representative of NLS1 in X-ray typical- and low-flux states, respectively. Therefore, it also follows that objects could transit from one sample to another depending on their X-ray flux state.

4 OPTICAL AND UV PROPERTIES

An advantage afforded with *XMM-Newton* is the availability of optical and UV data obtained with the Optical Monitor (OM; Mason et al. 2001) simultaneously with X-ray observations. For many of the NLS1 observations, OM imaging data were also collected at UV or optical wavelengths. Therefore, whenever possible, we determined rest-frame 2500 Å luminosities and optical-to-X-ray spectral indices (α_{ox}).

The standard definition of α_{ox} is: $\alpha_{ox} = \log(f_x/f_{uv})/\log(\nu_x/\nu_{uv})$, where f_x and f_{uv} are the intrinsic flux densities at 2 keV and 2500 Å, respectively; and ν_x and ν_{uv} are the corresponding frequencies. In many of the observations the rest-frame 2500 Å was directly observed within one of the OM broad-band filters. Consequently, the flux density at 2500 Å was estimated from the source count rate in that filter (Chen 2004). However, when this was not the case it was necessary to extrapolate from some measured UV wavelength (u) to 2500 Å. The modified expression for α_{ox} is then: $\alpha_{ox} = \log(f_x/f_u)/\log(\nu_x/\nu_u) + \log(f_u/f_{uv})/\log(\nu_u/\nu_{uv})$, where the second term on the right-hand side is the spectral slope between the measured UV flux density at u and 2500 Å. If measured by Constantin & Shields (2003), the source-specific value for the UV spectral slope was used (the value shown in Table 2). If the source-specific value was not known we adopted the spectral slope of the composite SDSS quasar spectrum between 1300 – 5000 Å ($\alpha_u = -0.44$; Vanden Berk et al. 2001).

The 2500 Å flux density was measured from the available pre-processed pipeline products for each source. For most observations, multiple images were taken in the same filter, in which case the average source count rate was used to estimate the flux densities (Chen 2004). For Mrk 1044, Mrk 896 and Mrk 493, images were only made in the V-band (5100 – 5800 Å). For these observations an extrapolation to 2500 Å was not done given that the optical spectra of AGN show a break in the continuum slope at about these wavelengths, which would introduce systematic uncertainties in the measurements of these three NLS1. Host-galaxy contribution was not excluded; thus will introduce a level of uncertainty in the reported values.

In addition, $\text{FWHM}(\text{H}\beta)$ and Fe II/H β ratios were collected from the literature for as many objects as possible. These are also included in Table 2.

¹ The X-ray flux of PG 1211+143 is also low compared to the *Ginga* observations (Lawson & Turner 1997).

Table 2. Optical and UV properties. The source name is given in column 1. The other parameters are the: 2500 Å flux density ($\times 10^{-26}$ erg cm $^{-2}$ s $^{-1}$ Hz $^{-1}$) (column 2); Fe II/H β (column 3); FWHM of H β (km s $^{-1}$) (column 4); UV flux density ($\times 10^{-26}$ erg cm $^{-2}$ s $^{-1}$ Hz $^{-1}$) (column 5); $\sim 1100 - 4000$ Å spectral index ($F \propto \nu^{\alpha_u}$) (column 6); and α_{ox} (column 7). Values in columns 5 and 6 are listed only when the 2500 Å flux density (column 2) was not directly available from the data.

General NLS1 Sample (S-sample)						
(1)	(2)	(3)	(4)	(5)	(6)	(7)
Source	f_{uv}	Fe II/H β	FWHM(H β)	f_u	α_u	α_{ox}
Mrk 766	0.57	1.56	1100	–	–	–0.958
Mrk 359	1.41	0.50	900	1.33	–0.44	–1.276
Mrk 1044	–	0.77	1310	–	–	–
Akn 564	1.31	0.67	865	–	–	–0.941
Mrk 896	–	0.50	1135	–	–	–
Mrk 335	5.43	0.62	1710	5.27	–0.64	–1.298
NGC 7158	–	–	2100	–	–	–
Mrk 493	–	1.16	800	–	–	–
I Zw 1	1.61	1.47	1240	1.20	–1.75	–1.170
Ton S180	4.40	0.90	970	3.88	–0.76	–1.417
PG 1448+273	0.98	0.94	1330	–	–	–1.407
UGC 11763	2.61	0.63	2210	–	–	–1.489
RX J0323.2–4931	0.17	0.65	1680	–	–	–1.131
Mrk 478	2.35	0.97	1630	–	–	–1.495
II Zw 177	–	–	1176	–	–	–
IRAS 13349+2438	1.06	1.25	2800	0.54	–3.23	–1.359
PKS 0558–504	–	1.60	1250	–	–	–
PG 1115+407	0.82	0.98	1740	0.84	–0.44	–1.371
Nab 0205+024	1.02	0.62	1050	1.03	–0.44	–1.340
PG 2233+134	0.53	0.89	1740	–	–	–1.407
E 1346+266	0.03	0.98	1840	–	–	–1.048
Complex NLS1 Sample (C-sample)						
NGC 4051	3.64	0.94	1170	–	–	–1.484
PG 1535+547	–	0.47	1480	–	–	–
1H 0707–495	1.54	2.77	1000	1.44	–0.46	–1.763
IRAS 13224–3809	0.65	2.40	650	0.60	–0.44	–1.536
PG 1211+143	2.89	0.50	1900	–	–	–1.517
PG 1402+261	1.87	1.10	1623	–	–	–1.441
PHL 1092	0.36	1.81	1300	0.30	–0.44	–1.560

5 MULTIWAVELENGTH PARAMETERS

In order to probe the multiwavelength behaviour of these NLS1 we collected various parameters from the literature such as: radio loudness, optical emission line strengths, C IV strength, black hole mass and Eddington luminosity ratios. Comparing the two samples in all parameter spaces possible with these data revealed no clear difference between the C- and S-sample; thus these parameters will not be considered further.

5.1 Contemporaneous X-ray and UV properties

Measurements of α_{ox} from simultaneous UV and X-ray data clearly demonstrate a difference in the slope of the optical-X-ray continuum in the two samples (Figure 2). The average index for the S-sample is -1.268 ± 0.179 compared to -1.550 ± 0.112 for the C-sample. A Kolmogorov-Smirnov (KS) test comparing the two distributions yields a probability of < 0.1 per cent that they are drawn from the same sample.

In Figure 2 we have plotted α_{ox} as a function of 2500 Å monochromatic luminosity. For comparison, the UV luminosity dependence of α_{ox} for radio-quiet, type 1 AGN ($\alpha_{ox} =$

$-0.136L_{uv} + 2.616$) is also shown (Strateva et al. 2005). The S-sample appears to follow this relationship relatively well, but most of the C-sample fall below the Strateva relation. In combination with the fact that the C-sample objects are in X-ray low-flux states (Section 3) this clearly demonstrates X-ray weakness in these complex objects during the observations.

For five NLS1 in the overall sample, at least two X-ray observations with contemporaneous OM data are available. Three of these objects (Ton S180, Mrk 478, Akn 564) are from the S-sample, the other two (1H 0707–495, NGC 4051) are from the C-sample. The epoch-specific α_{ox} and L_{uv} were calculated for each of these observations. The results are plotted in Figure 2 as crosses. For the objects in the S-sample, the fluctuations in α_{ox} are small and perhaps even negligible if a complete error analysis was considered.

In contrast, the α_{ox} variations are much more significant for the two objects in the C-sample (1H 0707–495 and NGC 4051). Figure 2 also indicates that the variations in α_{ox} are driven by changes in the X-ray flux, but that the UV flux also changes. For example, during the second observation 1H 0707–495 was about six times brighter in the X-rays, while its UV flux diminished by ~ 50 per cent. Increasing X-ray flux and decreasing UV flux was also seen in NGC 4051.

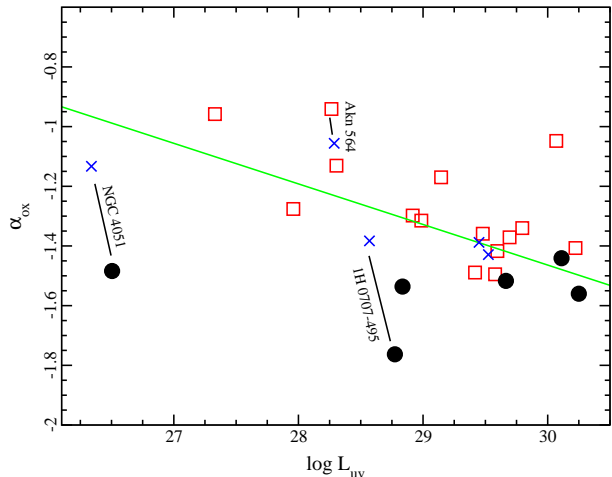


Figure 2. α_{ox} as a function of 2500 Å luminosity measured from contemporaneous X-ray and UV data. The filled (black) circles mark the C-sample NLS1 and the open (red) squares are the S-sample NLS1. For comparison, the relation $\alpha_{ox} = -0.136L_{uv} + 2.616$, found for radio-quiet type 1 AGN (Strateva et al. 2005) is shown as a green, solid line. The general NLS1 sample appears to follow the Strateva relation well, but the complex objects are X-ray weak. Multiple *XMM-Newton* observations exist for some of the objects in our sample. These are shown as blue crosses. The α_{ox} variations displayed by 1H 0707–495 and NGC 4051 indicate significant changes in the X-ray flux and more moderate variations in the UV. Akn 564 appears excessively X-ray strong, but this is likely due to reddening of the UV spectrum (Crenshaw et al. 2002).

We also note that in the second observations of 1H 0707–495 and NGC 4051, both objects portray simpler high-energy spectra. That is, the null hypothesis for a power law plus Gaussian fit for 1H 0707–495 and NGC 4051 at these epochs was 0.176 and 0.456, respectively. By our definition, neither object would have been considered ‘complex’ at those times, suggesting that when measured in ‘typical’ flux states, these source also follow the Strateva relation.

5.2 Optical properties

In Figure 3, the Fe II/H β ratio is plotted against the FWHM(H β). The average ratio for the S-sample is 0.93 ± 0.34 with modest scatter as indicated by the reported standard deviation. The average of the C-sample is 1.43 ± 0.91 with considerable more scatter. The two samples clearly overlap. From a KS-test it is determined that the probability that they are drawn from the same sample is 8 per cent. Although not highly significant there are indications that the strongest Fe II emitters are the ones that also display high-energy spectral complexity.

6 DISCUSSION

6.1 X-ray weak NLS1

According to Figure 2, objects that possess complexity in their 2.5 – 10 keV spectrum appear to be X-ray weaker (i.e. they are found below the average $L_{uv} - \alpha_{ox}$ relation). At least in two of the objects (NGC 4051 and 1H 0707–495) for which multiple, simultaneous, X-ray/UV observations are available, extreme epoch-to-epoch changes are seen in α_{ox} , demonstrating that when the spec-

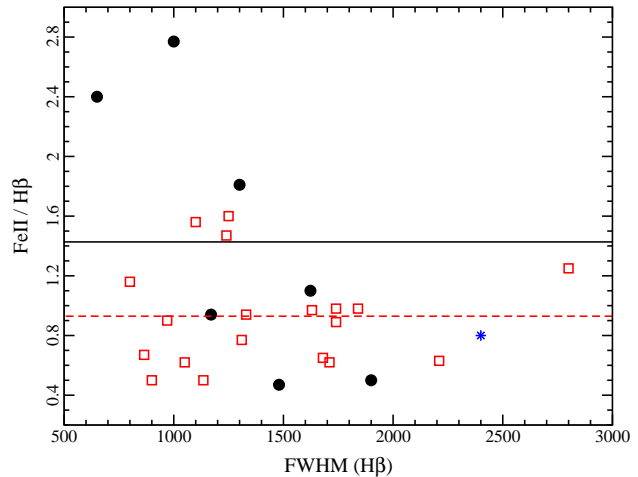


Figure 3. The Fe II/H β ratio is plotted against the FWHM(H β). The symbols are as defined previously. The average ratio for the S-sample (open squares) and the C-sample (filled circles) are marked by a dashed and solid line, respectively. Although there is considerably more scatter in the average ratio of the complex NLS1 sample, the objects appear to possess much stronger Fe II emission compared to H β . The average ratios are 0.93 ± 0.34 (general sample) and 1.43 ± 0.91 (complex sample). The sample is limited, but it appears the most extreme Fe II emitters (e.g. Fe II/H $\beta \gtrsim 1.7$) also display complexity in their high-energy spectra.

trum appears less complex, X-ray emission is stronger and α_{ox} is more typical.

The transiting of objects from the C- to the S-sample with increasing flux is predicted by both partial-covering and reflection models. In terms of partial-covering the increased spectral complexity during the low-flux states occurs because the intrinsic spectrum (presumably a blackbody plus power law) is highly absorbed, imposing edges and curvature in the detected spectrum. For reflection, the low-flux spectrum will likely be reflection dominated and the spectral curvature and drops will be associated with various reflection components (predominately the blurred iron line and soft excess; e.g. Ross & Fabian 2005).

6.1.1 Absorption

The X-ray weakness is, of course, in agreement with absorption models such as partial-covering where the X-ray emitting region is more absorbed than the UV region. This could occur, for example, if the absorber is located somewhere between the X-ray and UV emitting regions of the accretion disc. Consequently, UV fluctuations could arise from e.g. changes in the accretion rate, while the X-rays variations will appear larger because of the addition affect of the changing absorption. Therefore the extreme changes in the X-ray flux due to absorption can drive the fluctuations in α_{ox} when compared to the relatively unabsorbed and less variable UV flux. We also note that in the multi-epoch observations of 1H 0707–495 and NGC 4051 the UV flux diminished when the X-ray flux was higher.

A prediction of the partial-covering model (e.g. Tanaka et al. 2004) is that changes in the covering fraction or column density of the absorber(s) will account for, at least, the long-term spectral variations; but that the unabsorbed, intrinsic flux will remain relatively constant over time. We can test this prediction by reexamining the two *XMM-Newton* observations of 1H 0707–495 (Gallo

et al. 2004a). During both observations, the absorbed component of the intrinsic spectrum was seen through a column density of $\gtrsim 10^{23} \text{ cm}^{-2}$; however during the first, low-flux state observation the covering fraction² of the absorber was much greater. The intrinsic, 2 keV flux density during the first and second observation of 1H 0707–495 was 13.13 and $8.87 \times 10^{-30} \text{ erg cm}^{-2} \text{ s}^{-1} \text{ Hz}^{-1}$, respectively. This yields $\alpha_{ox} = -1.17$ at *both* epochs, demonstrating that a common intrinsic flux modified by partial obscuration is possible in accounting for the differences in brightness over time.

6.1.2 Reflection

Steep and fluctuating α_{ox} is not inconsistent with models, such as light bending (e.g. Miniutti & Fabian 2004), which incorporate general relativistic effects close to the black hole to account for some of the X-ray variability. In these models the low-flux, reflection dominated spectrum results when most of the emission from the primary, power law component is bent back toward the black hole and never reaches the observer. In comparison with the relatively constant UV emission (most likely produced by the colder accretion disc) α_{ox} will be smaller (X-ray weaker). As the emission from the power law continuum becomes important, the X-ray source becomes brighter and α_{ox} begins to flatten.

6.2 Optical Fe II emission

Not all of the NLS1 in the C-sample possess strong optical Fe II emission (specifically Fe II/H β), but it does appear that the most extreme Fe II emitters (e.g. Fe II/H $\beta \gtrsim 1.7$; IRAS 13224–3809, 1H 0707–495, PHL 1092) are spectrally complex.

Firm conclusions cannot be drawn due to the small number statistics, but this raises the possible conjecture that not all object which display complex X-ray spectra possess strong iron emission, but possibly all objects with extreme Fe II emission do possess the mechanism to create high-energy complexities. A simple test would be to make X-ray observations of a few extreme Fe II emitters, say with Fe II/H $\beta \gtrsim 1.7$, as suggested by Figure 3, and determine if their high-energy spectra are complex.

However, the fact that a source can transit from one sample to another depending on its X-ray flux state (Section 3) raises further issues and limits the conclusions we can make regarding Fe II emission. The primary issue is whether the Fe II emission is variable and if it depends on the X-ray continuum flux. There are several studies which show evidence for (e.g. Kollatschny & Fricke 1985; Kollatschny et al. 2000; Vestergaard & Peterson 2005; Wang, Wei & He 2005) and against (Goat et al. 1999; Kollatschny & Welsh 2001) significant Fe II variability. Since the Fe II measurements presented here are not contemporaneous with the X-ray measurements, we can only speculate on a possible connection between Fe II strength and X-ray spectral complexity.

An alternative possibility is that the strongest Fe II emitters simply show the greatest variability. If so, this makes it more likely to catch the strongest Fe II emitters in an extreme (low) flux state, as opposed to an average NLS1. IRAS 13224–3809, 1H 0707–495 and PHL 1092 are certainly known for their strong Fe II emission and significant variability. From the current analysis it is difficult to distinguish the two theories.

² Note that the covering fraction and column density are degenerate in partial-covering models and cannot be distinguished.

7 SUMMARY

We have investigated the nature of NLS1 which exhibit complexity in their high-energy (2.5 – 10 keV) spectrum. We identified seven out of twenty-eight NLS1 whose high-energy spectrum show significant deviations from a simple power law. We compared multi-wavelength properties of this complex sample of seven NLS1 with the larger sample to investigate whether we could identify any underlying physical processes that could be responsible for the spectral complexity. The main results follow.

- Considering long-term X-ray variability of the sources, the complex sample of NLS1 (C-sample) seems representative of objects in X-ray low-flux states, whereas the NLS1 in the general sample (S-sample) appear to be in a typical flux state.

- In cases where multi-epoch measurements of α_{ox} were possible, it appeared that α_{ox} approached more typical values as the complexity in the high-energy spectrum diminished. For 1H 0707–495 and NGC 4051 (both in the complex sample) the variations in α_{ox} were extreme and while predominately due to variability in the X-rays, the UV flux did also change. Specifically, in these two objects, the UV flux actually diminished when the X-ray flux was high and the spectral complexity less prominent. This is not inconsistent with either partial-covering or reflection scenarios.

- On average, the C-sample showed stronger Fe II emission (Fe II/H β) than the general sample. Specifically, the three most extreme Fe II emitters (with Fe II/H $\beta > 1.8$) of the twenty-eight NLS1, were all part of the C-sample of only seven. This raises an intriguing possibility that we may be able to identify complicated X-ray NLS1 based on the strength of the optical Fe II emission. It is not certain from this current analysis if the possible connection between X-ray spectral complexity and Fe II strength is due to high iron abundances or because strong Fe II emitters may exhibit greater X-ray variations and consequently are more likely to be caught in an extreme (low) flux state.

Both absorption and reflection models predict the observed behaviour in α_{ox} . It is interesting to note that in the case of 1H 0707–495 a common, intrinsic α_{ox} is predicted by the partial-covering model and is consistent with the *XMM-Newton* observations.

Partial-covering models make no strong assumption on the nature of the intrinsic spectrum, only that it is partly obscured. In this sense reflection models, which can describe the broad-band X-ray properties are attractive. While it seems obvious that reflection close to the black hole should occur it also seems premature to abandon concepts which employ absorption in the black hole environment to explain some of the X-ray behaviour.

ACKNOWLEDGEMENTS

Many thanks to Todd Boroson and Dirk Grupe for providing the black hole data. I am very gratefully to Thomas Boller, Niel Brandt, Andy Fabian, Günther Hasinger and Yasuo Tanaka for comments on the manuscript and many helpful discussions over the years. Much appreciation to the referee for a constructive report which has resulted in an improved paper. LCG acknowledges funding from the Japan Society for the Promotion of Science through a JSPS Postdoctoral Fellowship. Based on observations obtained with *XMM-Newton*, an ESA science mission with instruments and contributions directly funded by ESA Member States and the USA (NASA). This research has made use of the Tartarus (Version 3.2)

database, created by Paul O’Neill and Kirpal Nandra at Imperial College London, and Jane Turner at NASA/GSFC. Tartarus is supported by funding from PPARC, and NASA grants NAG5-7385 and NAG5-7067.

REFERENCES

- Arnaud K., 1996, in: *Astronomical Data Analysis Software and Systems*, Jacoby G., Barnes J., eds, ASP Conf. Series Vol. 101, p17
- Boller T., Brandt W., Fink H., 1996, *A&A*, 305, 53
- Boller Th. et al. 2002, *MNRAS*, 329, 1
- Boller Th., Tanaka Y., Fabian A., Brandt W. N., Gallo L., Anabuki N., Haba Y., Vaughan S., 2003, *MNRAS*, 343, 89
- Boroson T., Green R., 1992, *ApJS*, 80, 109
- Brandt W. N., Mathur S., Elvis M., 1997, *MNRAS*, 285, 25
- Brandt W. N., Boller Th., Fabian A., Ruzsokowski M., 1999, *MNRAS*, 303, 53
- Chen B., 2004, *XMM-Newton Calibration Documents* (CAL-TN-0019)
- Collin S., Joly M., 2000, *NewAR*, 44, 531
- Crenshaw D. et al. 2002, *ApJ*, 566, 187
- Constantin A., Shields J., 2003, *PASP*, 115, 592
- Comastri A., 2000, *NewAR*, 44, 403
- Crummy J., Fabian A., Gallo L., Ross R., 2006, *MNRAS*, 365, 1067
- Dewangan G., Boller Th., Singh K., Leighly K., 2002, *A&A*, 390, 65
- Dickey J. M., Lockman F. J., 1990, *ARA&A*, 28, 215
- Fabian A. C., Ballantyne D., Merloni A., Vaughan S., Iwasawa K., Boller Th., 2002, *MNRAS*, 335, 1
- Fabian A. C., Miniutti G., Gallo L., Boller Th., Tanaka Y., Vaughan S., Ross R. R., 2004, *MNRAS*, 353, 1071
- Gallo L. C., Tanaka Y., Boller T., Fabian A. C., Vaughan S., Brandt W. N., 2004a, *MNRAS*, 353, 1064
- Gallo L., Boller Th., Brandt W. N., Fabian A., Grupe D., 2004b, *MNRAS*, 352, 744
- Gierlinski M., Done C., 2004, *MNRAS*, 349, 7
- Goad M., Koratkar A., Axon D., Korista K., O’Brien P., 1999, *ApJ*, 512, 95
- Grupe D., 2004, *AJ*, 127, 1799
- Grupe D., Mathur S., 2004, *ApJ*, 606, 41
- Grupe D., Wills B., Leighly K., Meusinger H., 2004, *AJ*, 127, 156
- Jansen F. et al. 2001, *A&A*, 365, L1
- Joly M., 1987, *A&A*, 184, 33
- Kollatschny W., Fricke K., 1985, *A&A*, 146, 11
- Kollatschny W., Bischoff K., Dietrich M., 2000, *A&A*, 361, 901
- Kollatschny W., Welsh W. F., 2001, in: *Probing the Physics of Active Galactic Nuclei by Multiwavelength Monitoring*, Peterson B., Polidan R., Pogge R., eds, ASP Conf. Series Vol. 224 p 449
- Laor A., Fiore F., Elvis M., Wilkes B., McDowell J., 1997, *ApJ*, 477, 93
- Lawson A., Turner M., 1997, *MNRAS*, 288, 920
- Leighly K., Zdziarski A., Kawaguchi T., Matsumoto C., 2002, in: *Workshop on X-ray Spectroscopy of AGN with Chandra and XMM-Newton*, Boller Th., Komossa S., Kahn S., Kunieda H., Gallo L., eds, MPE Report 279, p. 259
- Leighly K., 2004, *ApJ*, 611, 125
- Leighly K., Moore J., 2004, *ApJ*, 611, 107
- Longinotti A., Cappi M., Nandra K., Dadina M., Pellegrini S., 2003, *A&A*, 410, 471
- Mason K. O. et al. 2001, *A&A*, 365, 36
- Mineshige S., Toshihiro K., Takeuchi M., Hayashida K., 2000, *PASJ*, 52, 499
- Miniutti G., Fabian A. C., 2004, *MNRAS*, 349, 1435
- Peterson B. M. et al., 2000, *ApJ*, 542, 161
- Pounds K. A., Reeves J. N., King A. R., Page K. L., 2004, *MNRAS*, 350, 10
- Pounds K. A., Reeves J. N., King A. R., Page K. L., O’Brien P. T., Turner M. J. L., 2003, *MNRAS*, 345, 705
- Proga D., Stone J. M., Kallman T. R., 2000, *ApJ*, 543, 686
- Puchnarewicz E. M. et al., 1992, *MNRAS*, 256, 589
- Remillard R., Schwartz D., Brissenden R., 1988, in: *ESA Proceedings of the Celebratory Symposium on a Decade of UV Astronomy with the IUE Satellite*, Vol. 2, p273
- Reeves J. N., Porquet D., Turner T. J., 2004, *ApJ*, 615, 150
- Reeves J. N., Turner M. J. L., 2000, *MNRAS*, 316, 234
- Reynolds C., Ward M., Fabian A., Celotti A., 1997, *MNRAS*, 291, 403
- Rodríguez-Ardila A., Viegas S. M., Pastoriza M. G., Prato L., 2002, *ApJ*, 565, 140
- Ross R. R., Fabian A. C., 2005, *MNRAS*, 358, 211
- Strateva I., Brandt W. N., Schneider D., Vanden Berk D., Vignali C., 2005, *AJ*, 130, 387
- Schmidt M., Green R., 1983, *ApJ*, 269, 352
- Strüder L. et al. 2001, *A&A*, 365, L18
- Tanaka Y., Boller Th., Gallo L., Keil R., Ueda Y., 2004, *PASJ*, 56, 9
- Uttley P., Fruscione A., McHardy I., Lamer G., 2003, *ApJ*, 595, 656
- Uttley P., Taylor R., McHardy I., Page M., Mason K., Lamer G., Fruscione A., 2004, *MNRAS*, 347, 1345
- Vanden Berk D. et al. 2001, *AJ*, 122, 549
- Vaughan S., Reeves J., Warwick R., Edelson R., 1999, *MNRAS*, 309, 113
- Veron-Cetty M., Veron P., 2003, *A&A*, 412, 399
- Vestergaard M., Peterson B., 2005, *ApJ*, 625, 688
- Wandel A., Peterson B. M., Malkan M. A., 1999, *ApJ*, 526, 579
- Wang J., Wei J., He X., 2005, *A&A*, 436, 417
- Yaqoob T., Serlemitsos P., Mushotzky R., Madejski G., Turner T., Kunieda H., 1994, *PASJ*, 46, 173

This paper has been typeset from a \TeX / \LaTeX file prepared by the author.